Science Advances

AAAS

advances.sciencemag.org/cgi/content/full/3/1/e1601992/DC1

Supplementary Materials for

Pure iron grains are rare in the universe

Yuki Kimura, Kyoko K. Tanaka, Takaya Nozawa, Shinsuke Takeuchi, Yuko Inatomi

Published 18 January 2017, *Sci. Adv.* **3**, e1601992 (2017)
DOI: 10.1126/sciadv.1601992

This PDF file includes:

Supplementary Text

Experimental System and Procedure

The nucleation chamber (n in fig. S2A) was a 150-mm-long stainless-steel cylinder with an internal diameter of 65 mm. It was equipped with two viewports for recording the paths of interference fringes of the two lasers, and one viewport for measuring the temperature of the evaporation source using a pyrometer (ISQ5-LO, Hazama Sokki Co. Ltd., Yokohama). Two ports were also equipped with a 0.1-mm-diameter chromel–alumel thermocouple [a combination of WF-1/8"PT -0.8-2-T -TK-1000 mm/150 mm (Tecsam Co. Ltd., Hsinchu) and KMT-100-100-050 (ANBE SMT Co., Yokohama)] for measuring the temperature at the end of the evaporation source as an alternative method for determining the temperature of the evaporation source. Two electrodes (PF-SM6-3KV-10A, Kawaso Texcel Co., Osaka) were used for heating the evaporation source. The chamber also had a specially coordinated high-resolution pressure gauge (HAV-60KP-V; Sensez Co., Tokyo). The accuracy of pressure measurement was ±90 Pa, which corresponds to an accuracy of ±1.5 K at the nucleation temperature (~900 K) given by our experimental results. A quarter-inch stainless steel tube (g in fig. S2A) was connected to a vacuum system through a valve (6LVV-DPBW4-P1; Swagelok Co., Manchester; va in fig. S2B) for evacuation and the introduction of gas. The air in the chamber was evacuated by a combination of a turbo-molecular pump (TG50F, 50 L/s; Osaka Vacuum, Ltd.) and a scroll-type dry vacuum pump (DIS-90; ULVAC Kiko Inc., Saito City). After a sufficient vacuum was attained (pressure 10^{-5} Pa), pure Ar gas (>99.9999% purity) was injected into the chamber. The Ar buffer gas was essential for measuring the partial pressure and temperature of evaporated Fe gas based on the shifts of interference fringes of optical lasers at two different wavelengths (see below). In addition, the inert Ar gas decreased the mean free path and shortened the cooling timescale of the evaporated Fe gas, which allowed us to perform the nucleation experiments within the short duration of the microgravity environment and within the limited space available in the rocket. To observe the effects of the Ar gas pressure on the results, the two nucleation chambers with identical configurations were installed in the rocket (fig. S2B) and each was filled with Ar gas at a different pressure (2×10^4 Pa and 4×10^4 Pa).

The Mach–Zehnder-type interferometer (fig. S2A) had two lasers: a polarized green laser with a wavelength λ_G = 532 nm (compact green laser module, 10 mW BEAM MATE HK-5616; Shimadzu Corp., Kyoto) and a red laser with a wavelength λ_R = 635 nm (4.5 mW continuous wave circular beam laser diode module; Edmund Optics Inc., Barrington, NJ). The evaporation source, a Fe wire (0.1 mmϕ × 100 mm) wrapped around a tungsten filament (0.3 mmϕ × 68 mm), was carefully aligned parallel to the optical path ($<4 \times 10^{-4}$ rad) and was made as long as possible to obtain a high column density of evaporated Fe gas. This enabled us to detect tiny changes in the refractive index of as little as 1.0×10^{-6}, which corresponds to a change in temperature from 298 K to 301 K for Ar gas at 2×10^4 Pa. Because the vapor pressure of metallic tungsten is much lower (10^{-5} Pa at 2508 K) than that of Fe (9.7×10^4 Pa at 2508 K), the partial pressure of evaporated metallic tungsten could be neglected during our experiments.

The interference fringes of the green and red lasers were captured by a recording system (Board Camera MS-88HCS without a low-pass filter; Moswell Co., Ltd., Yokohama) and were downloaded to the ground by telemetry at a rate of 10 frames per second during the experiment. The spatial resolution was ~45 μm.

Launch of sounding rocket S-520-28

Sounding rocket *S-520-28* of the Japan Aerospace Exploration Agency (JAXA) was launched at 4 pm JST on December 17th, 2012, and reached an altitude of 312 kilometers 283 seconds after liftoff. The mean gravitational acceleration during the parabolic flight, measured by a triaxial analogue accelerometer module (Model 2470-002; Silicon Designs Inc., Kirkland, WA) placed on a base plate of the nucleation chamber was $(6.3 \pm 0.8) \times 10^{-4}$ G (fig. S1), which is two orders of magnitude lower than that in microgravity experiments performed aboard aircraft. The duration of the microgravity was as much as ~445 seconds in this sounding rocket, much longer than the ~20 seconds achievable in aircraft. Such relatively long and better microgravity condition allowed us to perform two successive nucleation experiments at different Ar gas pressures (after waiting for residual convection to settle down) in a single flight. The rotational frequency of the rocket was kept as low as –0.018 Hz. Electrical heating of the evaporation sources in Ar gas at an initial pressure of 2.0×10^4 Pa (4.0×10^4 Pa) was performed for 65 seconds in total by constant elevation of the applied voltage (~0.13 V s^{-1}) between 180 and 240 seconds (255 and 315 seconds) after the launch, and at constant voltage at 8.6 V for the subsequent 5 seconds.

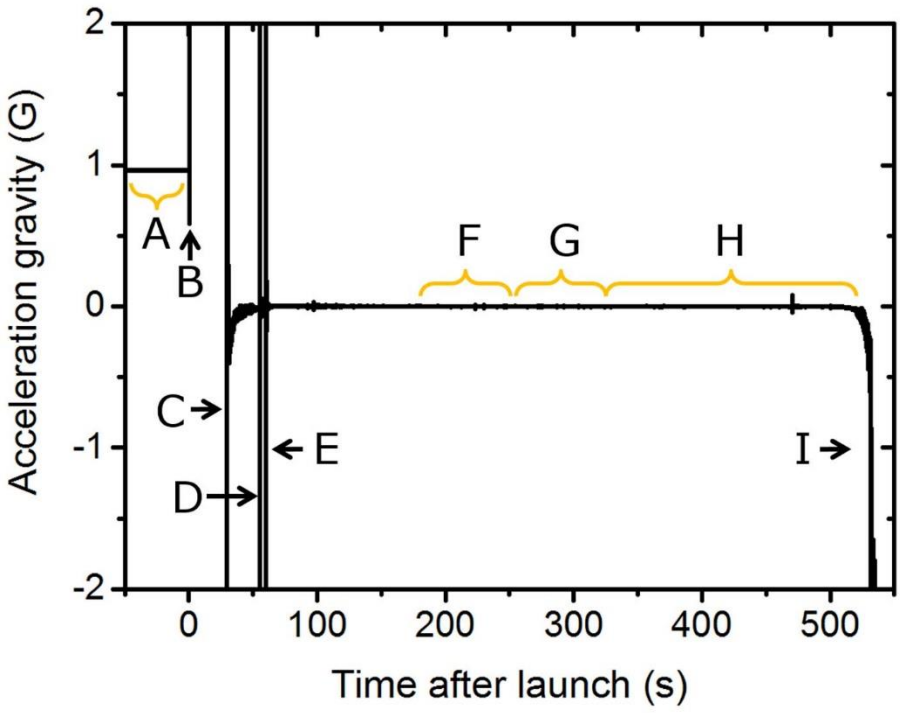

fig. S1. Time evolution of the acceleration gravity in the sounding rocket during the microgravity experiment. Labels **A** to **I** indicate the following events: A, before launch; B, launch; C, termination of ignition; D, despinning by spreading of yo-yo; E, opening of the nose cone for release of heat; F, experiment in Ar gas at 2.0×10^4 Pa; G, experiment in Ar gas at 4.0×10^4 Pa; H, transfer of the recorded images to the ground; and I, termination of parabolic flight. The gravitational acceleration was measured by a triaxial analogue accelerometer module positioned on the base plate of the experimental system. It was same order in three axes during parabolic flight.

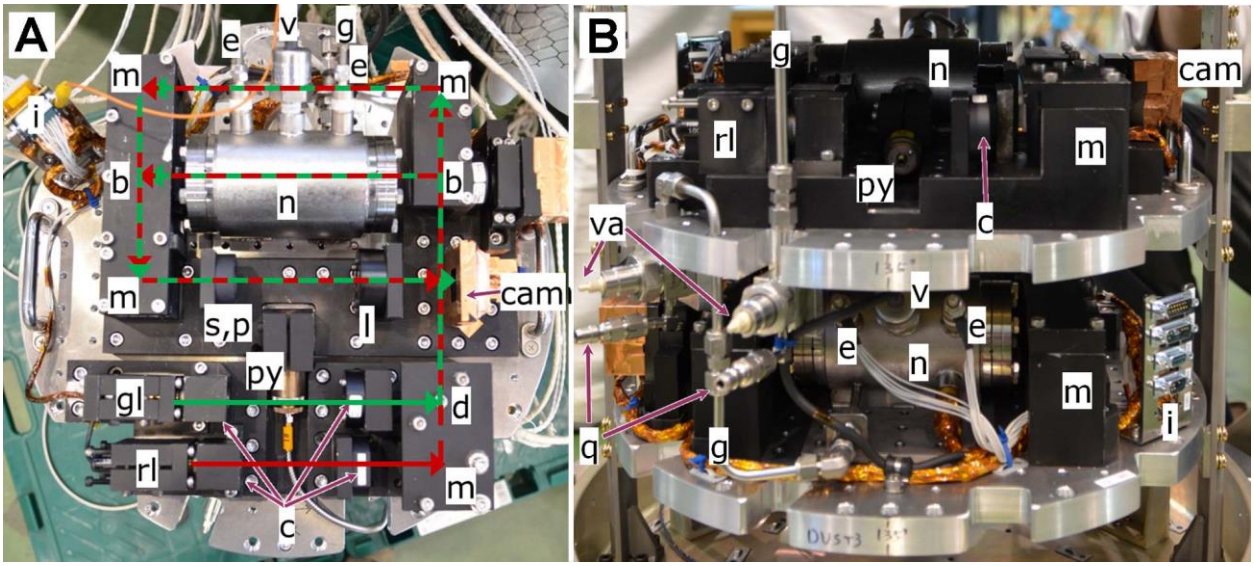

fig. S2. Photographs of the experimental systems. (**A**) Top view of the double-wavelength Mach–Zehnder-type laser interferometer with the nucleation chamber. Red and green arrows show the optical paths of red and green lasers, respectively. (**B**) Side view of the experimental systems. View directions of the upper and bottom systems are from bottom and top of A, respectively, i.e., each system is 180^{o} opposite in phase. Labels indicate: b, beam splitter; c, collimator; d, dichroic mirror; e, electrode; g, gas line; i, interface connecters; l, lens; m, mirror; n, nucleation chamber; p, polarizer; q, Quick-Connect; s, short-pass filter; v, vacuum gauge; cam, CCD camera; gl, green laser; rl, red laser; py, pyrometer and va, valve. Evacuation of the air and subsequent injection of Ar gas into the chamber were performed on the ground after the experimental system had been installed inside the rocket.

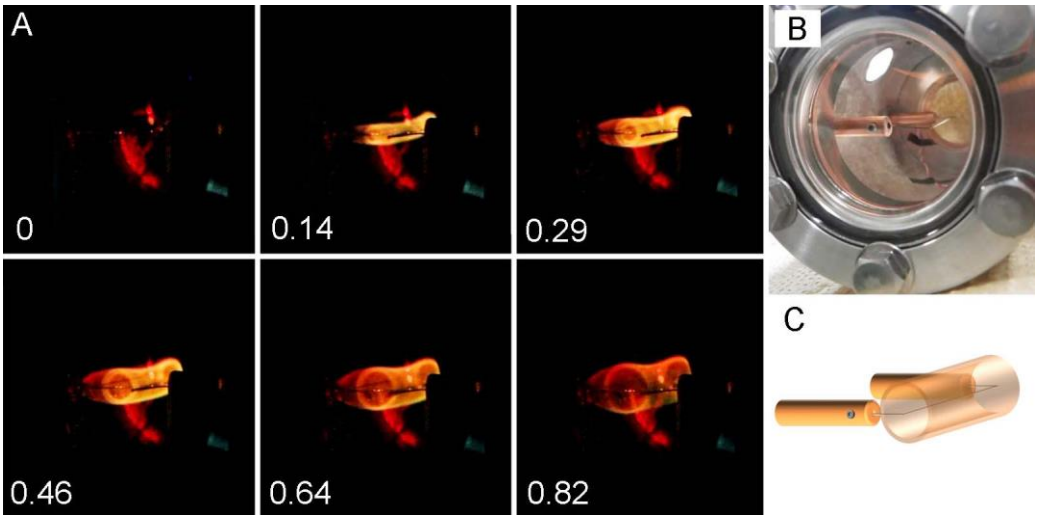

fig. S3. Examples of nucleated particles in a microgravity environment. (**A**) Real images obtained in another nucleation experiment of tungsten oxide during a parabolic flight of an aircraft of Diamond Air Service Inc., Japan. These images are shown to illustrate the existence of concentric nucleation around the entire evaporation source, which cannot be confirmed from the images of the interference fringes because the view direction is parallel to the evaporation source. The nucleated particles are illuminated by the hot evaporation source. Because the evaporation temperatures of Fe were very high, the bright evaporation source and the darker nucleated particles could not be recorded simultaneously due to the low dynamic range of our general camera. Tungsten oxide evaporates at a much lower temperature (~1200 K) than does Fe (~2000 K), permitting observation of its nucleated particles. The number in each image shows the time in seconds. The image in the upper left (labeled as 0) corresponds to an image recorded just before the appearance of nucleated particles. (**B**) Photograph of the chamber for the microgravity experiment in the aircraft from the same viewing direction as the panel A. (**C**) Schematic of the evaporation source and a smoke composed of nanoparticles. The smoke forms a concentric cylinder around the filamentary evaporation source because of symmetrical diffusion of the evaporated gas under microgravity.

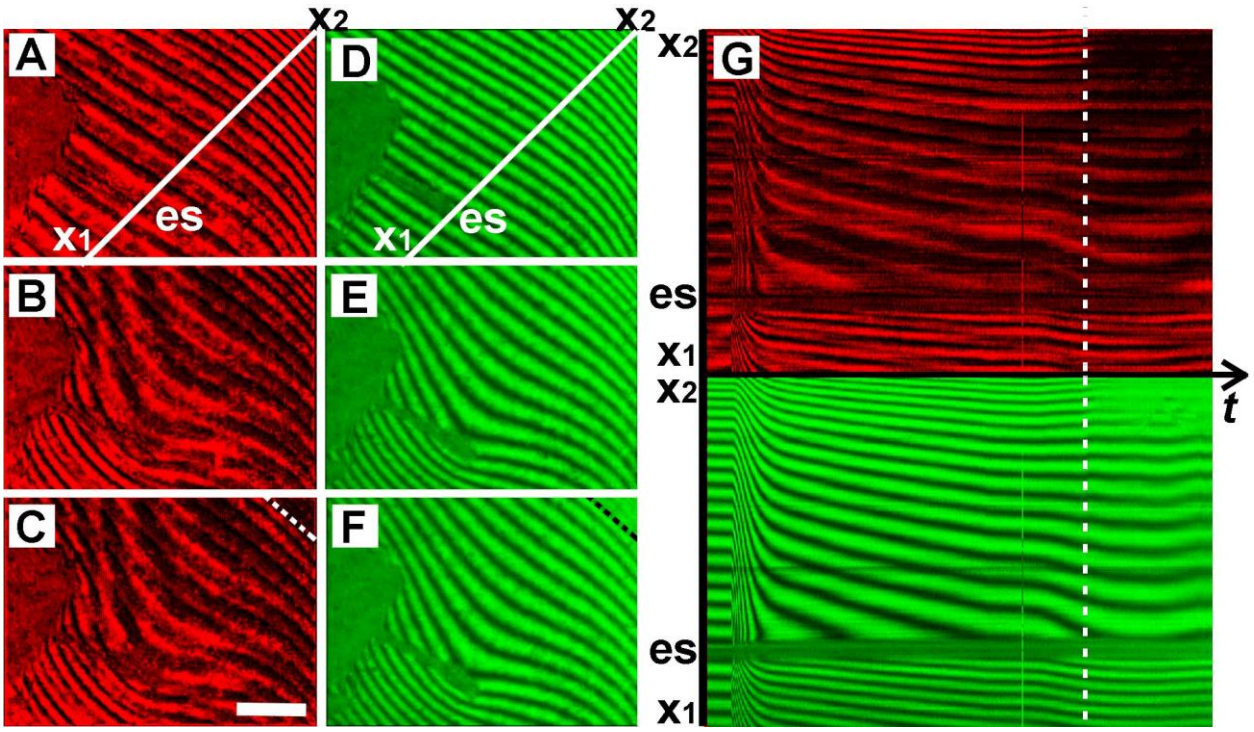

fig. S4. Images of interference fringes during the Fe nucleation experiment under microgravity. Color-separated images of the interference fringes in Fig. 2 for the red laser (**A**–**C**) and the green laser (**D**–**F**) at an initial Ar buffer gas pressure of 4×10^4 Pa: (A, D) before heating of the evaporation source, (B, E) 0.4 s before the nucleation of Fe grains and (C, F) at the time of nucleation. In C and F, the dotted line in the upper right corner indicates the nucleation front of the Fe grains, above which interference fringes disappear due to scattering of light by abundantly formed Fe grains. Panel (**G**) shows time-series images of the interference fringes indicated by white lines in A and D. Horizontal and vertical axes in the panels correspond to the time and position from x_1 to x_2, respectively. Labels es show the position of the evaporation source. The dotted white line in G shows the time of nucleation. The scale bar in C corresponds to 3 mm.